Assessment of moisture content profile in Douglas-fir wood using electrical resistivity-based tomography

Wael Hafsa, Tuan Anh Nguyen, Nicolas Angellier, Laurent Ulmet, Mokhfi Takarli, Octavian Pop, Frédéric Dubois

Assessment of a moisture content profile in Douglas-fir wood using electrical resistivity-based method

Wael Hafsa[a,*], Tuan Anh Nguyen[b], Nicolas Angellier[c], Laurent Ulmet[c], Mokhfi Takarli[c], Octavian Pop[c], Frédéric Dubois[c]

[a] *Aix-Marseille Université, CNRS IUSTI UMR 7343, Marseille, 13453, France*
[b] *Ho Chi Minh City University of Transport, Ho Chi Minh city, Vietnam*
[c] *Univ. Limoges, GC2D UR 14477, Egletons, F-19300, France*

Abstract

The service life and the durability of wood-based structures is closely related to the moisture content of the material. In order to establish an optimal and reliable evaluation of the moisture content distribution, this paper presents an experimental-numerical approach based on the adaptation of Electric Resistivity Tomography, mainly used for electrical prospecting measurements in geophysics. In this study, the method leads to identify a longitudinal resistivity profile by injecting electrical current and measuring the potential difference using needle-shaped probes inserted in a Douglas-fir sample. Numerical simulations of the moisture diffusion were carried out to validate experimental data of wood moistening process. Besides, a numerical approach based on a finite element method was set up to reproduce the electrical resistance measurements. A numerical inversion is sequentially implemented to minimize the gap between measurements and simulations of electrical resistances. The correlation between the numerical simulations of moisture content and the experimental results of electrical resistivity has been identified.

Keywords: Non destructive testing, Electrical resistivity, Wood, Moisture content

*Corresponding author
Email addresses: wael.hafsa@univ-amu.fr (Wael Hafsa), tuananh.nguyen@ut.edu.vn (Tuan Anh Nguyen), nicolas.angellier@unilim.fr (Nicolas Angellier), laurent.ulmet@unilim.fr (Laurent Ulmet), mokhfi.takarli@unilim.fr (Mokhfi Takarli), ion-octavian.pop@unilim.fr (Octavian Pop), frederic.dubois@unilim.fr (Frédéric Dubois)

1. State-of-the-art assessment

By taking into account today's main challenges in the decarbonizing construction, wood material has considerable advantages with regard to its environmental and ecological benefits [1]. The use of this material in construction and civil engineering applications raises new technical challenges in terms of performance-based durability design, i.e. the long-term behavior and the remaining useful life of timber structures [2, 3]. Nevertheless, the use of wood is hindered by durability issue related to the dependence relation between mechanical and physical properties and the in-situ service conditions. The development of fungal attacks requires a minimum moisture content of 20% and a temperature of 25 to 30 °C [4]. Therefore, biological attacks are more significant in outdoor structures subject to high humidity levels. By studying more than 245 large-span timber structures, Dietsch et al. [5] showed that damages usually depend on significant variations in the MC. As a result, maintenance strategies should be organized to develop inspection and monitoring methods destined for controlling moisture content in wooden structures. In this context, nondestructive testing (NDT) methods are presented as one of the solutions for the assessment of MC for timber structures. Several techniques were investigated by several studies for example :

- The near-infrared spectroscopy by characterizing the surface chemical changes in response to moisture uptake and loss in wood [6].

- The gammadensimetry by applying gamma-type electromagnetic radiation which is a method applied in the laboratory [7].

- The Ground Penetrating Radar (GRP) by propagating electromagnetic waves of frequencies between 300 megahertz and 300 gigahertz [8] in order to evaluate the dielectric constant : this technique is characterized by a sensitivity to electrode size, bonding pressure and the presence of cracks [9].

- Electrical method to evaluate the material resistance or conductance by injecting electrical current into wood/electrode surface ; this method is mainly integrated into the in-situ measurement strategies [10, 5] and requires a consideration of the effect of temperature variation [11].

In order to evaluate wood MC using electrical method, different electrodes types were used. Bjorngrim et al. [12] have proposed to place stainless steel thread between the glulam beams while Li et al. [13] have used copper patches as electrodes. Moreover, the use of needle-shaped probes and pins pressed against the material, or inserted into it, are very popularly used thanks to the ease of instrumentation. In fact, an European standard has been produced for Commercial instruments for a MC between 7 and 30% [14]. For this MC range, and at a constant temperature, the wood electrical resistance R (also valid for resistivity ρ which is an intrinsic property of the material) decreases as it MC (denoted w) increases according to Eq. (1), where E and F are two material constants [15].

$$ln(R) = E + F\ ln(w) \tag{1}$$

Nevertheless, the techniques mentioned above are generally suitable for yield local measurements and they are limited to the element surface [16]. Hence, such solutions remain impractical for providing more general information to evaluate the MC distribution for a timber building element, i.e. the moisture gradient which could cause differential shrinkage and increase crack risk [17, 18]. For those reasons, this work suggests to employ the Electric Resistivity Tomography (ERT), also known as the electrical imaging generally used in geophysics, and to adapt it to wood material. In geophysics, by injecting a direct current (DC) into the ground, ERT allows the development of a 3-dimensional survey based on the intrinsic electrical properties of soil (resistivity and chargeability due to the polarization of the medium). By using electrical geophysical imagery, many research works have been applied to semi-infinite mediums to study the features of a hydrocarbon contaminated site [19], to detect buried quarry and soil cracks [20] and to study the internal structure of volcanoes [21]. In order to evaluate resistivity fields, experimental measurements are generally coupled with numerical modeling by assuming a surface point current injection. Verdet et al. [22] showed that the electrode finiteness should be considered in case of small-scale ERT surveys. An inversion procedure based on optimization methods is also applied to minimize the differences between experimental and numerical modeling results. Among these methods, the least-squares optimization method of Gauss-Newton or Levenberg-Marquardt are the most common [23].

In recent years, ERT has been adapted for applications on finite mediums, for example to investigate the health state of reinforced concrete structures

by identifying corrosion risk [24]. This technique has also been adapted to characterise non-destructively the distribution of metallic fibres in concrete [25]. For on-site applications, ERT has been performed in a reinforced concrete wharf using embedded multi-electrode sensors to determine the correlation between the evolution of the compressive strength and the electrical resistivity [26]. In the past few decades, electrical imaging has been also integrated into wood applications. Most of works focuses on the determination of electrical resistivity of living trees by placing electrodes around the tree trunk [27, 28]. Such applications have shown interesting results helping forestry managers to detect certain diseases pre-symptomatically [29, 30]. However, after the passage of a wooden element through drying until construction, ERT is still under-explored area when MC is in the hygroscopic range, i.e. $0\% < \text{MC} <$ Fiber Saturation Point (FSP) about 25 to 30% for most species). In this context, our study presents a novel approach based on the adaptation of ERT. This resistivity-based method has been used to identify a longitudinal MC gradient throughout a Douglas-fir sample, which can have a major influence on crack behavior of a wood element This species is widely planted in France, and its use in construction is a part of the Neo Terra regional road-map dedicated to the energy and ecological transition of the $Nouvelle - Aquitaine$ region [31].

Fig. 1 presents a thorough overview of our proposed approach by considering both the numerical and experimental strategies. As first part of this study, the measuring tool has been adapted to wood material characterized by high resistivity ranges [32]. Electrical resistance measurements take into account the injected current I_{AB} (between two electrodes A and B) and the difference in potential V_{MN} (between two electrodes M and N). Measurements have been sorted according to both wood properties and resistivity-meter performance (Q_{Th}). In order to determine numerical resistance R_{num}, this work proposed to perform a finite element modeling (FEM) and to simulate the current injection by using thermal-electrical analogy. To evaluate resistivity values (ρ_{exp}) all along the sample, numerical inversion was necessary to ensure the transition from geophysical conditions to wood material conditions. The results of numerical and experimental resistances were sequentially coupled to fed numerical inversion based on Levenberg-Marquardt algorithm. In addition, as the material wets, a finite difference method (FDM) is used to simulate wood moisture diffusion process. The diffusion parameters were optimized by using Simplex algorithm. Finally, the results of electrical resistivity and moisture content were mixed to identify the transition relationship.

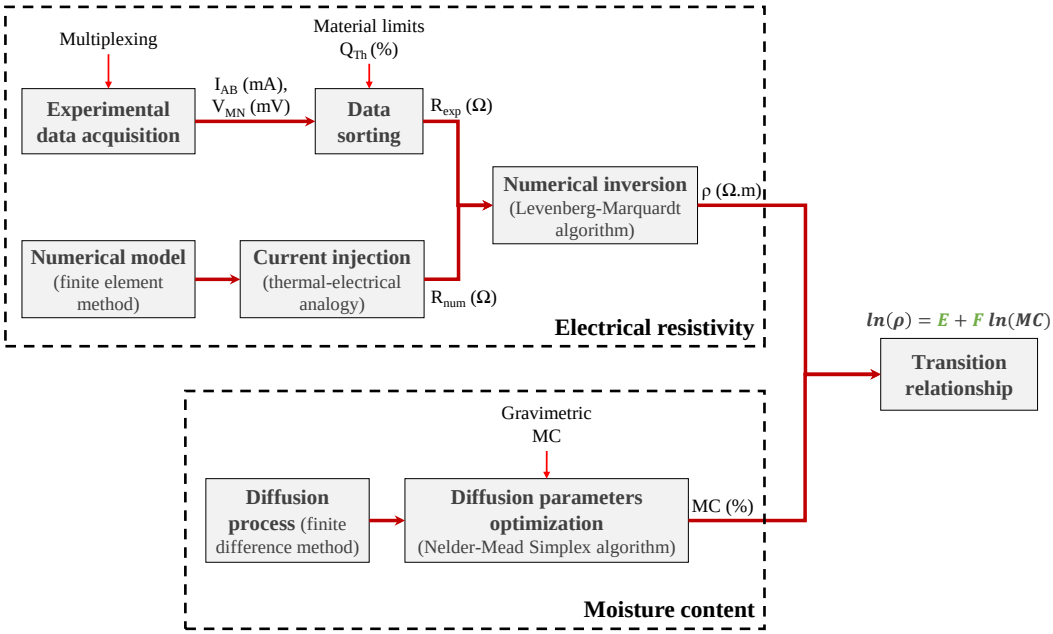

Figure 1: Overview of the mixed experimental-numerical approach

2. Experimental protocol

2.1. Sample preparation and conditioning

Measurements were performed on a Douglas-fir (Pseudotsuga menziesii) sample and the dimensions were 320 x 95 x 95 mm^3. The sample was produced according to the fiber directions (L : Longitudinal, R : Radial and T : Tangential). An overview of the sample preparation is presented in Fig. 2.

The choice of the geometry is a compromise allowing to install 21 electrodes based on non-insulated needle-shaped probes (1 mm radius). Electrodes were numbered from 1 to 21 and were lined up along the longitudinal direction in the upper face (LT) and parallel to the fiber orientation. They were set at a depth of 10 mm with a 15 mm distance between them. The sample was initially conditioned at a relative humidity RH = 40%, and then 2 layers of parafilm were set up on 5 of the 6 faces in order to perform a unidirectional longitudinal diffusion. The homogeneity of moisture content distribution as well as the electrical resistivity over the cross section, has been assumed. This diffusion process allows the evaluation of a unidirectional moisture gradient. The one-dimensional moisture transfer reproduces the reality of wooden structures when the ends of the beams are subjected to

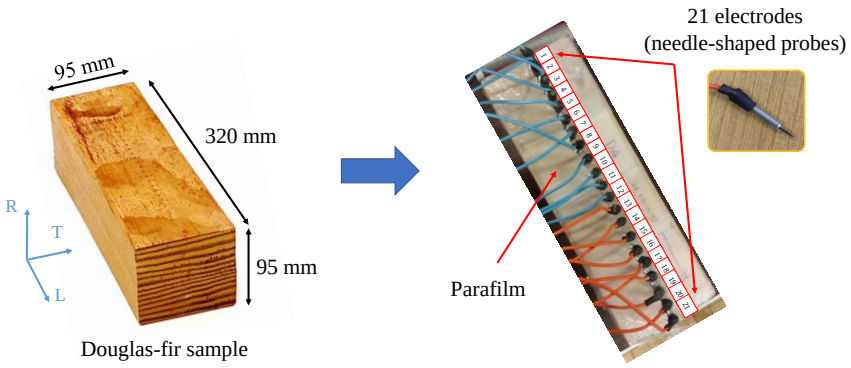

Figure 2: Preparation of Douglas-fir sample

uniaxial diffusion. The sample was then placed in a desiccator over saturated potassium-chloride-based salt solution (37.2 g/l of (K-Cl) to achieve a RH of 86%. The average ambient temperature of the room in which the desiccator has been installed was approximately about 20 °C. The room temperature was not controlled, thus, variations of ± 2 °C were observed throughout the experiment. However, we assume that these small variations will not put into question the application of the proposed method [33]. The specimen was stored for an extended conditioning period (over 3 years) and weights data have been collected during this period. After oven drying, the sample was weighed to determine its anhydrous mass. The average gravimetric MC is then calculated at each step according to Eq. (2), where m_w is the mass of the wet specimen and m_0 the specimen's oven-dry mass.

$$MC_{grav}(\%) = \frac{m_w - m_0}{m_0}\ 100 \tag{2}$$

The initial MC was estimated at $w_{ini} = 10.6\%$. The evolution of the average MC vs. conditioning period is shown in Fig. 3. It is important to note that the recording of electrical resistivity measurements was considered since 217 days from the humidification process initiation – i.e. by taking into account the reliability of measurements, no significant data were observed before, and high deviations were noted due to the operational limits related to the dry wood. Thus, electrical measurements were conducted from the 217^{th} days and then at 245, 287, 313, 352, 398, 457, 537 and 1092 days.

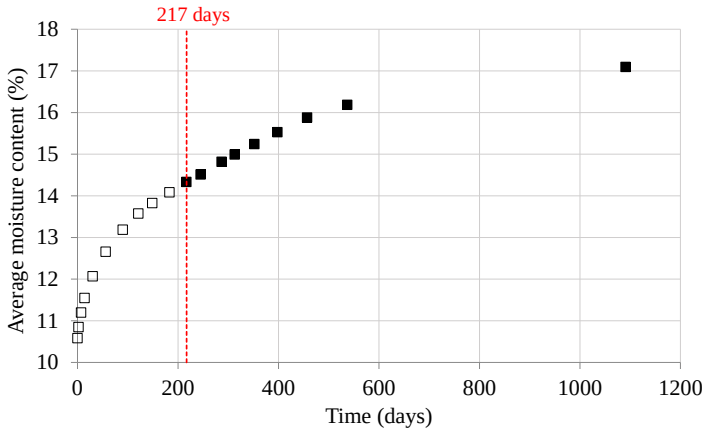

Figure 3: Evolution of average moisture content, where filled squares denote that electrical resistivity measurement is effective (after 217 days)

2.2. Principle and material adaptation for resistance measurements

The resistivity-meter used in this study is a *Syscal Junior Switch 48* from *Iris Instruments*. The principle of this Megohmmeter is based on the use of the quadrupole electrode configuration. By applying a high DC voltage, an electrical current of intensity I_{AB} is transmitted between two injection electrodes (A and B) and the resulting difference in potential V_{MN} between the other two electrodes (M and N) is measured, as shown in Fig. 4.

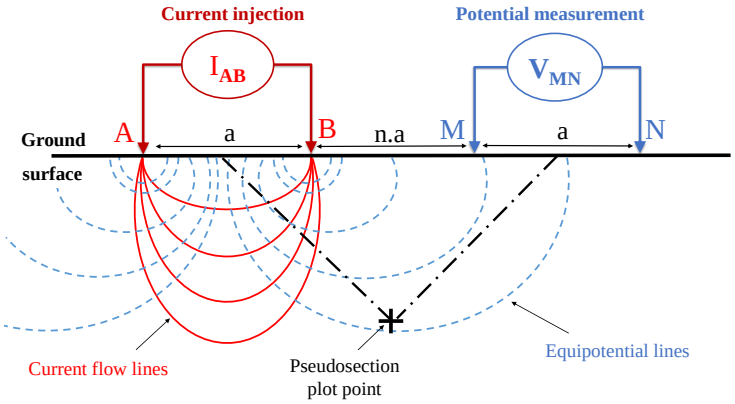

Figure 4: The principle of apparent resistivity measuring used in geophysics: current injection and voltage measuring (example of Dipole-Dipole configuration)

In geophysics, the resistivity-based method defines the apparent electrical resistivity ρ as a function of two inversely proportional parameters R and k (Eq. 3), which represent respectively the electrical resistance (in Ohms) and the geometric coefficient (in meters) corresponding to each configuration and depending on the distance between electrodes (a). The electrical resistance represents the medium's nature and the geometric coefficient represents the electrode device used.

$$\rho\ (\Omega m) = k\ R = k\ \left|\frac{V_{MN}}{I_{AB}}\right| \tag{3}$$

Depending on the positions of electrodes A, B, M and N, several configurations can be defined. Each configuration is different in terms of the measurement noise sensitivity, the resolution quality and the investigation depth. A primary parametric study has shown that Dipole-Dipole configuration represents a good measurement repeatability and an efficient current injection [33]. Besides, this configuration has been chosen in this study thanks to its low electromagnetic coupling due to the distance separation between the current and potential lines [23].

The standard deviation coefficient Q allows us to estimate the resistance measurement error, so the measurement's quality. In fact, it represents the dispersion around the mean value of resistance $\bar{R}$ during S measures. The number of measures S is fixed by the operator and depends on the updated value of Q. In our case, 3 measurements are made at least. If Q is greater than 5%, 6 measurements will be made, as described in Eqs. (4 - 5 - 6).

$$Q(\%) = \frac{100}{\bar{R}}\ \sqrt{\frac{1}{S}\sum_{i=1}^{S}(R_i - \bar{R})^2} \tag{4}$$

where,

$$\bar{R} = \frac{1}{S}\ \sum_{i=1}^{S} R_i \tag{5}$$

$$S = \begin{cases} 3 & \text{if } \ Q \leq 5\% \\ 6 & \text{if } \ Q > 5\% \end{cases} \tag{6}$$

Fig. 5 presents a thorough overview of the experimental protocol. The material adaptation to wood applications has been processed in four main steps :

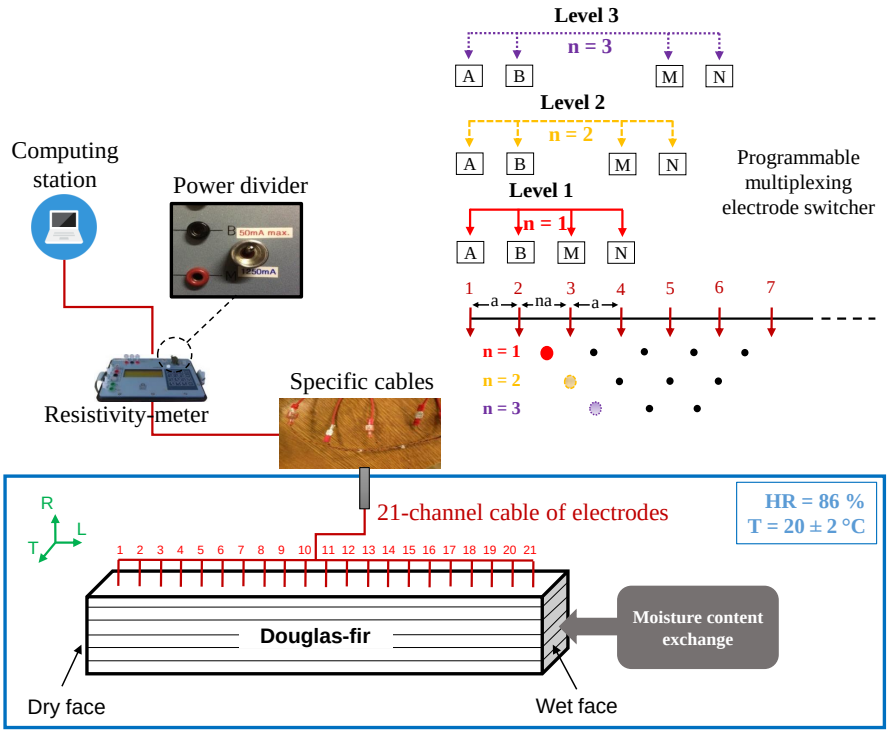

Figure 5: Experimental protocol and programmable multiplexing electrode switcher

- In geophysics configuration, the maximum applied potential can reach ± 400V corresponding to a maximum injected intensity of 1.25 A. The range of the measurable potential V_{MN} is chosen by the user. Since wood is characterized by a very high electrical resistance, this parameter was set up to its maximum value ;

- Specific cables and miniaturized electrodes were manufactured ;

- Since the resistivity-meter had originally been developed for geophysical applications, a current divider module was integrated providing a usable voltage measurement. The current injection and resolution ranges were modified from 1.25 A to 50 mA and from 10 μA to 0.4 μA, respectively ;

- A parametric study showed that long duration of voltage application allows to reach the equilibrium of the voltage V_{MN} and to avoid the

polarization of the electrode-wood contact surface [34]. A maximum injection duration of 2 seconds was then set up.

The programming of measurement sequences and multiplexing pattern were developed by using Electre II software. The recorded measurements were stored in the built-in memory and then transferred by means of a serial link (Prosys software) to an external computing station for the data processing and interpretation steps (Res2DInv software in geophysics). The conditioning desiccator was modified to insert the resistivity-meter cables, thus, measurements were performed by keeping the sample inside. Electrical resistance data were obtained using the 21-channel cable. In order to obtain a resistivity mapping, the use of an internal multiplexing system allows to control the used electrodes by modifying the distance between injection and measuring electrodes. Multiplexing was carried out using three levels of investigation depths $n = \{1, 2, 3\}$. For each level, a horizontal scan has been performed by taking into account $a = 15$ mm as a reference distance between electrodes. By considering the 3 investigation depths, 51 experimental measurement points are possible. Fig. 6 shows the example of the electrical resistance measurements obtained after 1092 days. The measurements have

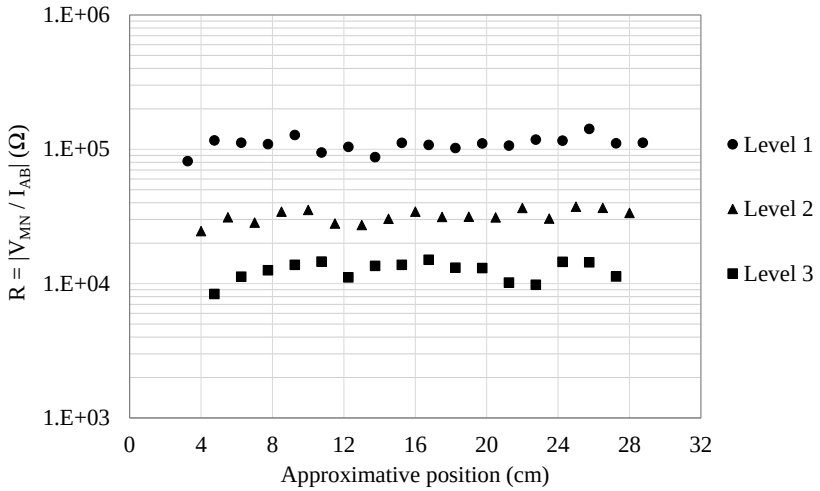

Figure 6: Measurements of electrical resistances at 3 investigations levels (after 1092 days)

shown the capacity of the multiplexed electrical method to dissociate three resistance levels in accordance with the investigation depths.

3. Numerical approaches

The aims of the numerical part of this work are : (i) to solve the differential equations related to moisture diffusion, and (ii) to develop an inversion strategy based on finite element model (FEM) not restricted to conventional geophysics assumptions, i.e. two-point injection into a semi-infinite medium.

3.1. Moisture diffusion process

The moisture diffusion is defined through the nonlinear Fick's second law, as described in Eq. (7). This equation is valid for a transient wetting process where D (in m^2/s) is the diffusion parameter that depends on the moisture content.

$$\frac{\partial w}{\partial t} = D_w \frac{\partial^2 w}{\partial x^2} \tag{7}$$

According to isothermal conditions, the mass transfer process integrates a relationship based on non-linearity between moisture content level and orthotropic diffusion tensor. For a uniaxial representation characterized by x coordinates, the spatial-temporal differential equation can be written as follows [35] :

$$\frac{\partial w}{\partial t} = \frac{\partial}{\partial x}(D_w \frac{\partial w}{\partial x}) \tag{8}$$

To take into account the exchanges between water vapor molecules and bound water molecules in wood cells, it is commonly considered to employ a virtual exchange layer defined by an instantaneous equilibrium between external fibers and water vapor in the neighboring climatic environment. This equilibrium is usually driven by sorption hysteresis and defined by the virtual moisture content value, called w_e and obtained at constant conditions of temperature and RH [36, 37]. Solving Fick's equation requires also to integrate the surface moisture content. Thus, by taking into account the boundary conditions on the surface Ω, the diffusion equation can be expressed as follows :

$$D_w \frac{\partial w}{\partial x} = S(w_e(t) - w_\Omega(t)) \tag{9}$$

where S and w_Ω represent the hydrous surface exchange coefficient and the moisture content values at the surface Ω, respectively.

For a unidirectional and nonlinear isothermal diffusion process, an exponential form is used to represent the impact of moisture content on the diffusion coefficient in wood materiel [38] :

$$D_w = D_0 \exp(k\ w) \tag{10}$$

where D_0 is the anhydrous diffusion coefficient in (m^2/s), and k is a constant representing the non-linearity of the phenomenon (positive in the radial and tangential directions, and negative in the longitudinal direction).

The differential equation representing the diffusion in the current part of the sample, can be written in the following form :

$$\frac{\partial w}{\partial t} = D_0 \exp(k\ w)\left[k\left(\frac{\partial w}{\partial x}\right)^2 + \frac{\partial^2 w}{\partial x^2}\right] \tag{11}$$

Finite difference method is considered as a suitable method for uniaxial moisture diffusion problems [7]. Numerical method based on FDM has been developed using Microsoft Visual Basic to solve differential equations.

3.2. Spatial-temporal MC profiles

The next step has been proposed to define the spatial-temporal moisture distribution throughout the sample. Let's consider the sample conditioned at initial moisture content w_{ini}. From time $t = 0$, an ambient virtual moisture content w_e is imposed on the non sealed face, as shown in Fig. 7.

An uni-directional diffusion transfer is assumed according to the thickness of the sample and following the main directions of the wood, i.e. the moisture flow is then oriented along the x axis. The sample is discretized into slices of equal thickness, perpendicular to the x axis, and each point corresponds to a specific mean value of moisture content of each slice. The time discretization is based on an explicit Euler scheme [39, 40] considering the time step τ. Let's denote w_i^t the moisture content at time t and at position i. The temporal integration allows to deduce the evolution of moisture content at position i as follows:

$$w_i^{t+\tau} = \big(1 - \frac{2}{M}\big)w_i^t + \frac{1}{4M}\big[k\big(w_{i+1}^t + w_{i-1}^t\big)^2 + 4\big(w_{i+1}^t + w_{i-1}^t\big)\big] \tag{12}$$

where :

$$M = \frac{\Delta x^2}{D_0\ \tau\ exp(k\ w_i^t)} \tag{13}$$

On the surface, if the limiting conditions are of Newton's type, the vapor concentration is established by convective transfer modeled by an exchange law as Eq. (9). The surface moisture content is then written as follows :

$$w_n^{t+\tau} = \frac{2}{M} w_{n-1}^t + \left(1 - \frac{2}{M - \frac{2}{N}}\right) w_n^t + \frac{2}{N} w_e \tag{14}$$

where :

$$N = \frac{\Delta x}{S\ \tau} \tag{15}$$

The surface exchange coefficient of the sealed face is considered to be zero. From Eq. (14), the moisture content becomes:

$$w_n^{t+\tau} = \frac{2}{M} w_{n-1}^t + \left(1 - \frac{2}{M}\right) w_n^t \tag{16}$$

As shown in Fig. 7, by knowing moisture content value at time t, the moisture content to the edge at time $t + \tau$ can be predicted. When the sample's moisture content profile is known at time $t = 0$, we then can calculate the moisture content for each point at next time $t + \tau$. For a given time, the moisture content of each slide is updated step by step. Finally, an iterative time process allows to update the temporal field of moisture content. This approach has been validated by several comparison tests with spatial moisture content profiles available in the bibliography, and also with spatial measurements of moisture contents made by the gammadensimetry method [7].

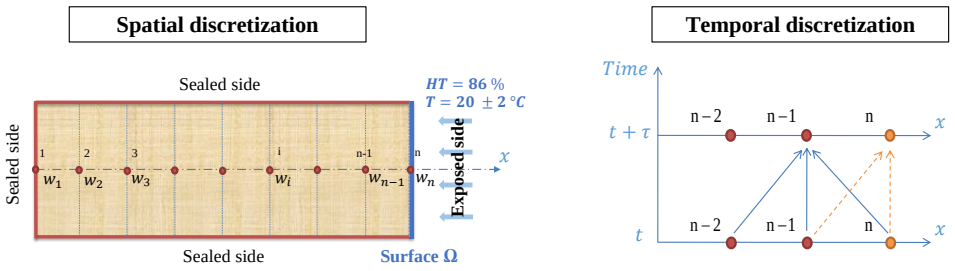

Figure 7: Spatial and temporal discretizations of the sample

3.3. Diffusion parameters optimization

As a reminder, the initial moisture content $w_{ini}(\%)$ of the sample has been determined by weighing for ambient RH. The diffusion parameters that need to be determined in this study, are summarized as follows : the virtual moisture content $w_e(\%)$, the anhydrous diffusion coefficient $D_0(m^2/s)$, the surface exchange coefficient $S(m/s)$ and the non-linearity constant k. In the aim of achieving an optimal solution taking into account these parameters, an inversion algorithm based on the simplex method is used in order to minimize the difference between the average moisture contents : the experimental one obtained by weighing and the numerical one obtained by the FDM. This optimization is based on a Nelder-Mead Simplex algorithm aiming to minimize the least squares-based difference between the sample's average MC measured during the experimental test $\bar{w}_{exp}$ and the calculated MC $\bar{w}_{num}$ using FDM. The objective function is denoted f et can be written as in Eq. (17), where N is the total number of measurements and t_i denotes the i^{th} measurement time.

$$f = \frac{1}{N}\sqrt{\sum_{i=1}^{N}\left(\bar{w}_{num}(t_i) - \bar{w}_{exp}(t_i)\right)^2} \tag{17}$$

From a numerical standpoint, with respect to the sample length called L, the average moisture content $\bar{w}_{num}$ is calculated according to Eq. (17) where w_{num} is calculated using FDM and defined at each point.

$$\bar{w}_{num}(t) = \int_L w_{num}(x,t)dV \tag{18}$$

The simplex method [41] consists of minimizing the objective function using only function values and without calculating the derivative. Taking into account the four unknowns (D_0, S, k and w_e), this method considers a geometric polyhedron, called simplex, composed of 5 nodes, with each node representing a unique solution. Based on a hierarchy of errors for each solution, this algorithm reduces the geometric surface until convergence is reached. The vertices of this polyhedron will undergo geometric transformations in moving towards a global minimum [42]. The simplex algorithm iterations correspond to simple algebraic operations on the polygon vertices for elementary geometric transformations (m_r for reflection, m_{ec} and m_{ic} for external or internal contraction respectively, m_e for expansion and m_s for

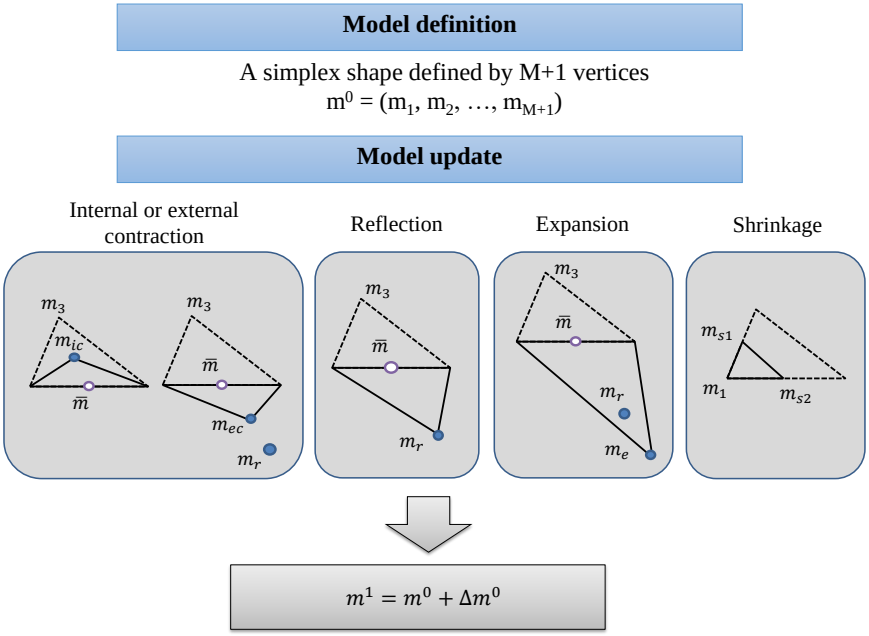

Figure 8: Flowchart of the Simplex Algorithm

shrinkage) [43], as shown in Fig. 8. Each iteration transformation solely depends on a series of comparisons between objective function values corresponding to the calculated points and values of the polygon vertices to replace the worst vertex (maximum) by the new fixed point. The polygon is thus reflected, extended or reduced depending on the function shape until its optimum corresponds to a complete reduction of the simplex yielding the optimal solution.

3.4. Resistivity-based numerical inversion

In order to determine the resistivity values associated with the resistance measurements, the aim of this study is to develop an inversion strategy based on a numerical model that is not restricted to the standard geophysics assumptions (point injection in a semi-infinite medium). That's why, the actual sample dimensions and the geometry of electrodes should be taken into account. The finite element software *Cast3m* has been employed to develop the numerical model [44]. As a first simplified approach, the assumption of an isotropic model has been employed. This assumption has yielded good

results for small dimension samples in a laboratory scale [33]. As shown in Fig. 9, the strategy is based on 3 main steps :

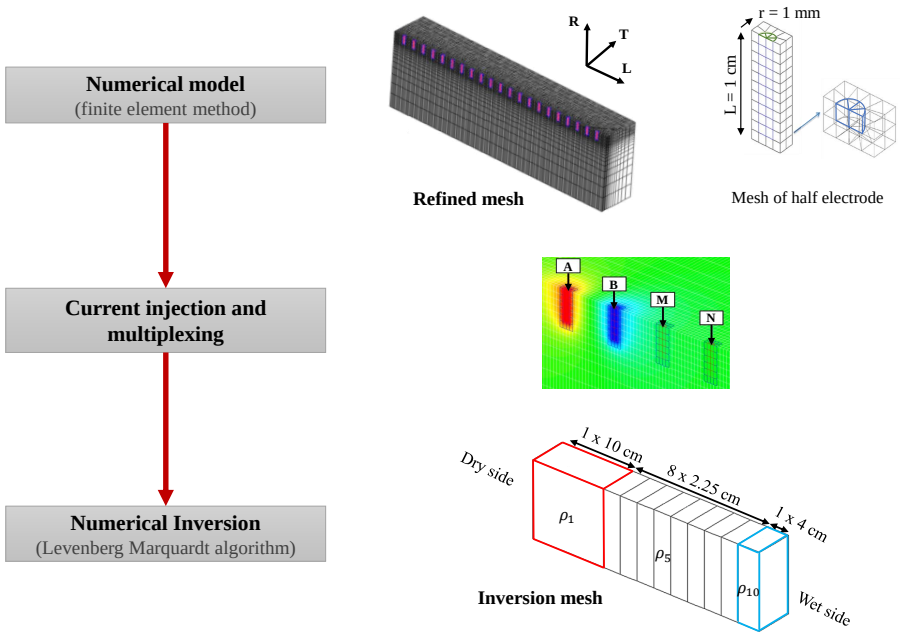

Figure 9: Numerical model, multiplexing and inversion

Numerical direct model. Only half-samples have been discretized due to the symmetry of the experimental configuration. As a first step, electrodes used for both current injection and potential measurement, have been modeled as semi-cylinders (1mm radius and 10 mm length) characterized by a high electrical conductivity of 1E3 $\Omega^{-1}m^{-1}$. The discretization of the sample volume has been developed according to the sample's geometry and by preserving electrodes installation areas. A refined mesh has been adapted for an accurate forward calculation. In order to increase the current injection resolution, the discretization was further refined around the electrodes and the mesh size has been gradually increased until the sample size has been reached. Finally, electrodes have been placed and connected to the sample.

Current injection and multiplexing. Taking into account the multiplexing procedures defined in the experimental protocol, the simulation of the measurements combines current injection and potential calculus. The current

injection has been established according to the ohm's law resolution (Eq. 19) where J is the current density ($A.m^{-2}$), σ is the electrical conductivity (S/m) and V is the measured voltage (V).

$$\overrightarrow{J} = -\sigma \overrightarrow{grad}\,(V) \tag{19}$$

The material response to current injection is analogous to heat transfer process described by the Fourier's law (Eq. 20), where φ is the heat flux density ($W.m^{-2}$), λ is the thermal conductivity ($W.m^{-1}.K^{-1}$) and T is the temperature (K).

$$\overrightarrow{\varphi} = -\lambda \overrightarrow{grad}\,(T) \tag{20}$$

The current injection has been generated by delivering a current density (1A intensity) from the electrode surface to the electrode-wood contact surface. In accordance with the linear Ohm's law, the resistance value remains independent of potential or injected current.

Numerical inversion. The inverse resolution of the direct model serves to deduce the resistivity properties of the studied medium by use of an optimization algorithm that minimizes the differences between measured and calculated resistance values. In order to determine the distribution of resistivity in the longitudinal profile of the sample, the assumption of constant resistivity in the transverse direction has been employed. That's why, an inversion mesh has been defined by discretizing the sample into 10 elements of variable widths ($\rho_1, \ldots, \rho_{10}$) where each element is assigned to a homogeneous resistivity value. The inversion mesh was coarser in the edges represented by ρ_1 (the dry side) and ρ_{10} (the wet side). Between the edges, the area is divided into 8 equal width slices of 2.25 cm. This type of discretization has been employed to recover at least one measurement in the wet side, and to improve the reliability of measurements in the dry side. The coarse-meshed resistivity field is then projected into the refined mesh to calculate the electrical resistance.

The numerical inversion strategy relies on the identification of M electrical conductivity m_i with $i = \{1, ..., M\}$. The investigated medium is discretized by a grid with a constant conductivity in each cell, as represented by a vector $m = (m_1, m_2, ..., m_M)$ used to deduce resistivity such as :

$$m_{resistivity} = \left(\frac{1}{m_1}, \frac{1}{m_2}, ..., \frac{1}{m_M}\right) \tag{21}$$

The measured resistances are considered as a data vector $d = (d_1, d_2, ..., d_M)$, with N depending on the multiplexing. The direct problem is then defined as a function $f(m)$, whose result is a vector compound of calculated resistances from the direct model. The resolution of an inverse problem calls for optimizing model parameters in order to minimize the difference between measured and calculated data, yielding to the following objective function:

$$F = (\Delta d - J\Delta m)^T.(\Delta d - J\Delta m) \tag{22}$$

$$\Delta d = d - f(m_0) \tag{23}$$

where Δd represents the difference between measured and calculated data. The inversion results converge on the correction of the initial model m_0 by a perturbation Δm. The NxM coefficients of the Jacobian matrix represent the measurement sensitivity at one point to a variation in model parameters and are calculated by approximating the derivative:

$$J_{i,j} = \frac{f_i(m_j + \Delta m_j) - f_i(m_j)}{\Delta m_j} \tag{24}$$

This inversion model relies on the Levenberg-Marquadt algorithm [45], i.e. according to the following expression:

$$\Delta m = (J^T J + \lambda W_m)^{-1} J^T \Delta d \tag{25}$$

where W_m is an MxM identity matrix. This model includes a damping factor λ that allows for convergence to a realistic solution, which is used dynamically: the first iteration is performed with a high enough value (1E16) compared to the high terms of the Jacobian matrix. For later iterations, the perturbation Δm is calculated with either a decrease $\alpha(0.2)$ or an increase $\beta(10)$ of the damping factor with respect the objective function evolution. The matrix inversion is directly conducted using a Gaussian elimination with partial pivoting. The stop criterion f_m, set at 1E-3, is based on the parameters variation between two successive iterations:

$$\left| \frac{m_{i+1} - m_i}{m_i} \right| \leq f_m \tag{26}$$

4. Results and discussions

4.1. Identification of diffusion parameters

Based on the approaches described in Sect. 3.1 and 3.3, simulations based on diffusion modeling were conducted to determine numerically the evolution of average moisture content in the sample. The diffusion parameters are presented in Table 1.

Table 1: Diffusion parameters

Parameters	Results
$D_0(m^2/s)$	3.02E-09
k	-5.23
$S(m/s)$	5.63E-07
$w_{ini}(\%)$	10.6
$w_e(\%)$	17.4

As shown in Fig. 10, results shows a good superposition between average moisture contents obtained by weighing and the evolution of numerical average moisture content based on FDM. In fact, the determination of the anhydrous mass by weighing allows to estimate initial MC and the equilibrium MC is adjusted by the presence of experimental data near equilibrium. Numerical simulations were also performed by taking into account the diffusion coefficients corresponding to the initial and the final (until moisture content equilibrium) hydric states denoted $D_{w_{ini}}$ and D_{w_e} respectively. Results confirm that the mass transfer process depends on the degree of moisture content of the material and the relationship between D and MC is illustrated in Fig. 11.

The moisture dependence shows the variation of D from 1.73E-9 to 1.22E-9 m^2/s within the range of moisture content increasing from 10.6 to 17.4 %. Results show a coherence as regards the to various works carried out to identify the diffusion coefficient of different wood species in the longitudinal direction for example : 1.8E-9 for Pinus sylvestris [46] and 1.04E-9 for Abies [47]. Otherwise, the above results confirm the non-linearity of diffusion process in the longitudinal direction with a negative coefficient k $\neq$ 0. The process is characterized by a low surface exchange coefficient S symbolizing

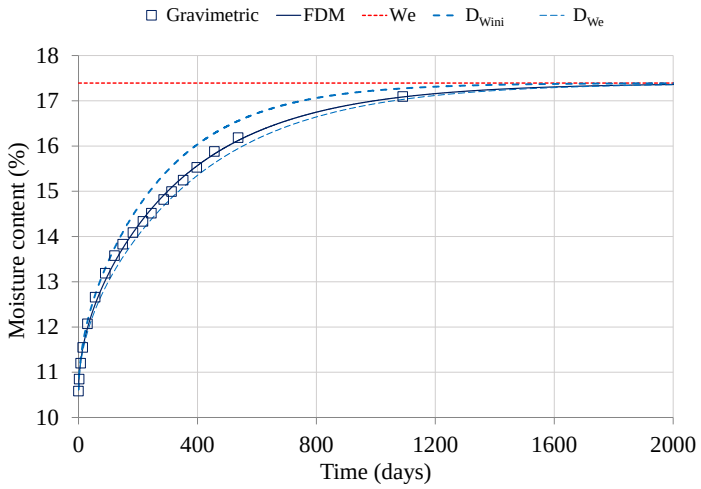

Figure 10: Comparison between moisture contents determined by gravimetric and FDM methods

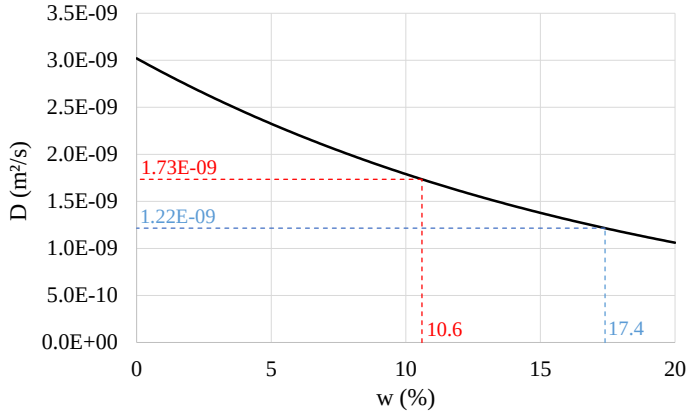

Figure 11: Evolution of diffusion coefficient

the superficial resistance for moisture transfer being equivalent to a wood's thickness of 2 to 3 mm.

Based on the optimized diffusion parameters, the spatial-temporal moisture content profiles are developed throughout the sample (Fig. 12). The distribution of the moisture content throughout the sample shows a clear gradient from the dry side to the wet side. Results show a moisture content

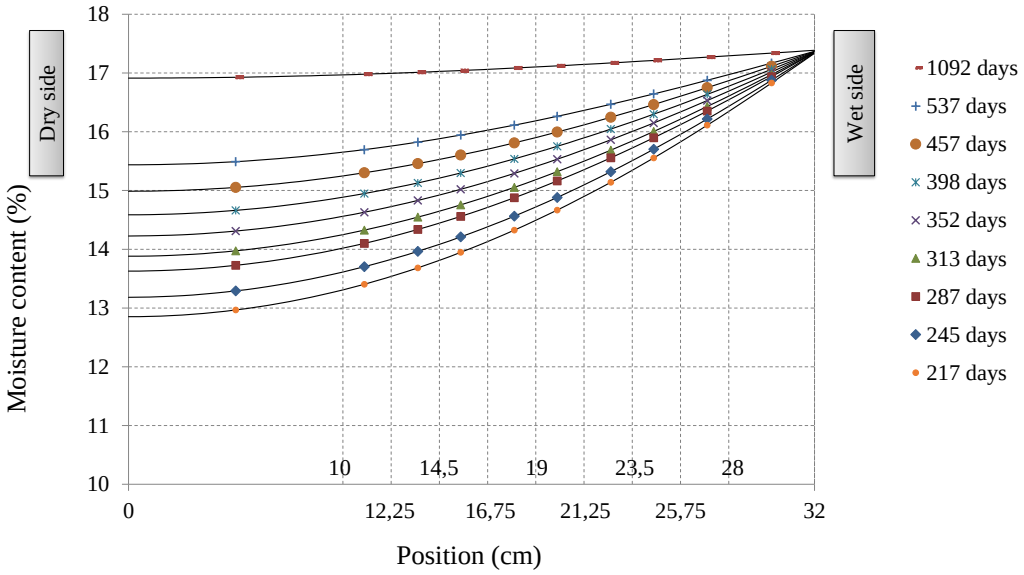

Figure 12: Numerical results of temporal spatial profiles of moisture content

range from 12.97 % to 17.34 %. The gradient decreases over the duration of wetting process. After 1092 days, the calculated MC values shows a relatively small variation which suggests overall coherence as regards the homogeneity of the moisture content distribution in the sample. The question rises how long does it takes to get a uniform distribution throughout the sample. The electrical resistivity measurements were set up in an effort to answer this question. Electrical and MC profiles will be then mixed to establish a transition relationship between resistivity and MC.

4.2. Identification of electrical properties

By taking into account 3 investigations levels, the identification is based on the comparison of the electrical resistivity profiles obtained throughout the experiment with the identified numerical MC spatial profiles. As shown in Fig. 13, the numerical model satisfactorily aligns with measurements by yielding a low error especially at the end of the humidification process when the electric current is easily injected.

The numerical inversion results, presented in Fig. 14, confirm that the resistivity gradient evolves from the dry side to the wet side of the sample in the longitudinal direction. The range of electric resistivity goes from

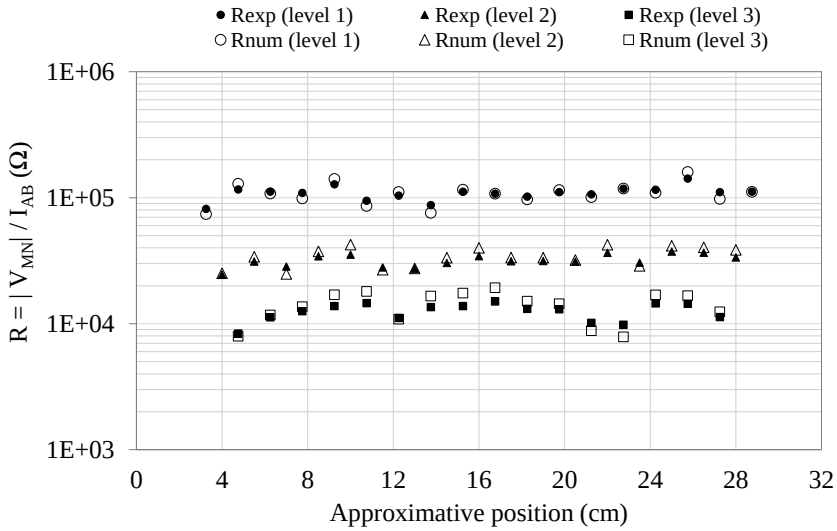

Figure 13: Experimental and numerical results of electrical resistances profiles for 3 investigations levels (after 1092 days)

3.66E+04 to 3.13E+05 $\Omega.m$.

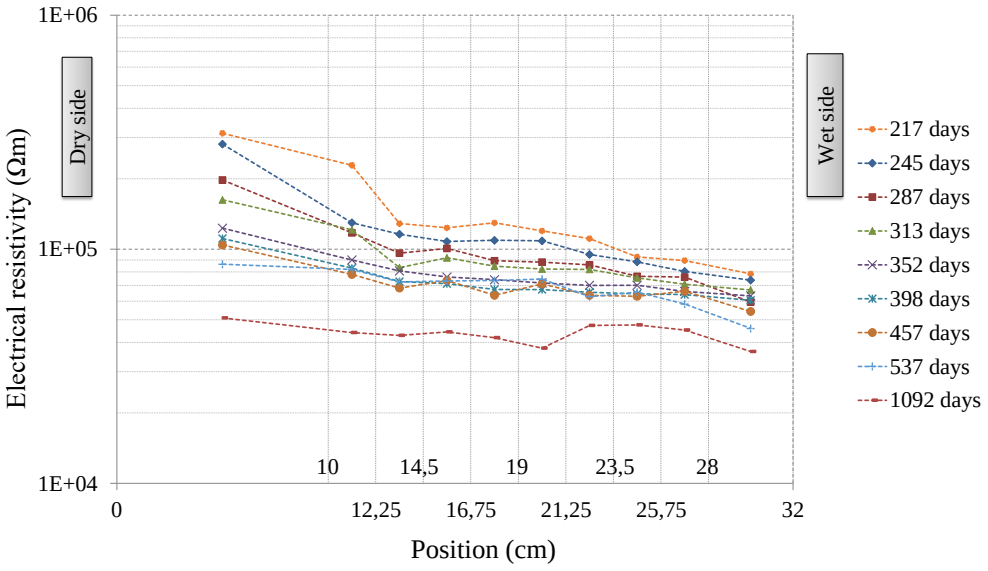

Figure 14: Temporal spatial profiles of electrical resistivity

The distribution of the resistivity throughout the sample shows a clear gradient from the dry to the wet side. These results are consistent with MC simulations by showing a homogeneous resistivity after 1092 days.

4.3. Determination of transition relationship parameters

Results presented in Sect. 4.1 and Sect. 4.2 will be mixed here to identify the transition relationship between resistivity and moisture content. In fact, at constant temperature, the transition law, linking the resistivity profiles to the corresponding moisture content profiles, is determined by linear regression in order to evaluate the parameters E and F, as described in Eq. (1). This identification is based on two methods as shown in Figs. 15 and 16.

Global identification. This approach is based on the use of all spatio-temporal data of resistivities and moisture contents where the linear regression results present a slope $F = -4.94$ for a MC range from 13 to 17.3%. This represents the variation coefficient of resistivity vs. moisture content.

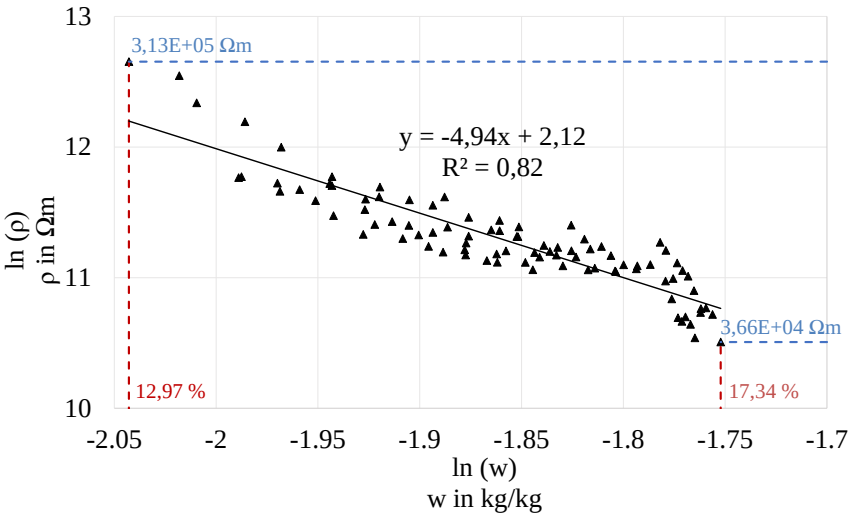

Figure 15: Global identification of transition law parameters

The negative value of F confirms that resistivity decreases with an increase in moisture content. This global trend confirms also that below the PSF, the presence of moisture is mainly located in cell walls in the form of bound water. This trend is different in the case of free water present in the cell cavities [48].

Weighted identification. In order to balance the weight of the resistivity measurements, the data are weighted according to a moisture content step of 0.5%. This approach conducts then to identify $F = -6.25$. This result is consistent with the studies applying electrical resistance measurements on softwoods species where Stamm [49] found $F = -5.99$ for *Pinuse-elliottii* (5<MC<32%) and Yamamoto [48] found $F = -6.12$ for *Araucaria-hunsteinii* (6<MC<25%). These comparisons confirm the hypothesis given by several

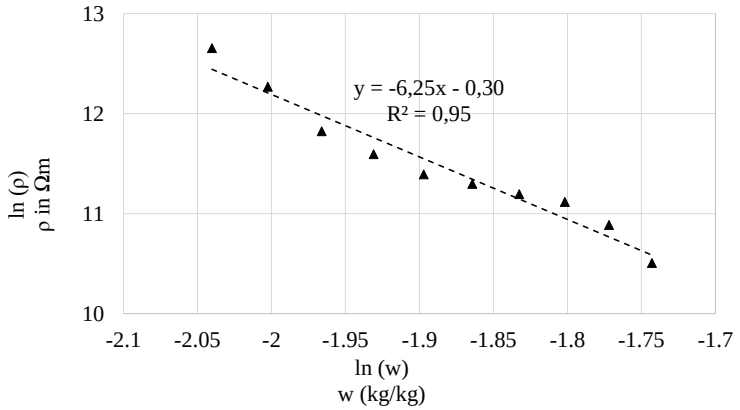

Figure 16: Weighted identification of transition law parameters

studies assuming that the parameter F is quasi-constant among wood species [50, 51]. Furthermore, no significant effect of the change of the dimensional scale is observed comparing to the results of a parametric study performed on small Douglas-fir samples (50 x 50 x 50 mm^3) where $F = -6.01$ [34].

5. Conclusions

As mentioned in the bibliographic state-of-the-art, the durability of wood material is often affected by the influence of climatic conditions i.e. the service classes assigned to wood structures. In this paper, an original experimental-numerical approach has been proposed to investigate moisture adsorption process within the range of moisture content from 13 to 17.4 % for a Douglas-fir sample. The developed method is based on multiplexed electrical resistivity measurements and the following conclusions can be drawn:

- A useful guideline is provided for monitoring electrical resistivity gradient in the longitudinal direction. In order to simulate the electrical

injection, a finite element model has been developed and coupled to a robust data inversion method.

- An exponential-based model has been used to characterize the moisture diffusion process in wood. Results have shown a good agreement between experimental data and simulations based on difference finite method leading to a realistic moisture gradient.

- The relationship between electrical resistivity and moisture content was defined at a constant temperature by using an empirical model.

The question rises how long does it takes to get a uniform distribution over the cross section in radial and tangential direction and how big is the influence of the gradient on the stress-strain-behavior. In addition, further improvements have to be considered for in-situ investigations:

- Taking into account the effect of temperature (direct radiation), wind and rain.

- Improving experimental acquisition in dry climatic conditions which create problems of current injection and high electrical resistivities due to low moisture content (<13%).

- Evaluating the effect of orthotropy by placing electrodes in the tangential and the radial directions of fibers.

6. Declaration of Competing Interest

The authors declare that they have no known competing financial interests or personal relationships that could have appeared to influence the work reported in this paper.

References

[1] L. Valentin, M. Dabbagh, M. Krarti, Benefits of switchable insulation systems for residential buildings in france, Energy and Buildings (2022) 111868.

[2] J.-W. Van de Kuilen, Service life modelling of timber structures, Materials and Structures 40 (1) (2007) 151–161.

[3] M. Riggio, M. Dilmaghani, Structural health monitoring of timber buildings: A literature survey, Building Research & Information 48 (8) (2020) 817–837.

[4] L. Reinprecht, Biological degradation of wood., Wood deterioration, protection and maintenance (2016) 62–125.

[5] P. Dietsch, A. Gamper, M. Merk, S. Winter, Monitoring building climate and timber moisture gradient in large-span timber structures, Journal of Civil Structural Health Monitoring 5 (2) (2015) 153–165.

[6] M. Awais, M. Altgen, M. Mäkelä, T. Belt, L. Rautkari, Quantitative prediction of moisture content distribution in acetylated wood using near-infrared hyperspectral imaging, Journal of Materials Science (2022) 1–14.

[7] T. A. Nguyen, N. Angellier, S. Caré, L. Ulmet, F. Dubois, Numerical and experimental approaches to characterize the mass transfer process in wood elements, Wood Science and Technology 51 (4) (2017) 811–830.

[8] T. C. Mai, S. Razafindratsima, Z. M. Sbartaï, F. Demontoux, F. Bos, Non-destructive evaluation of moisture content of wood material at gpr frequency, Construction and Building Materials 77 (2015) 213–217.

[9] X. Zhang, Surveillance et auscultation des ouvrages en bois par identification des champs hydrique et mécanique: Couplage des méthodes acoustiques et electromagnétiques, Ph.D. thesis, Université de Limoges (2021).

[10] C. Brischke, A. O. Rapp, R. Bayerbach, Measurement system for long-term recording of wood moisture content with internal conductively glued electrodes, Building and Environment 43 (10) (2008) 1566–1574.

[11] W. Hafsa, N. Angellier, M. Takarli, O. Pop, Monitoring of timber structures: moisture content evaluation by using electrical resistivity method, in: 5th International Conference on Structural Health Assessment of Timber Structures, 2019, pp. 658–70.

[12] N. Björngrim, P.-A. Fjellström, O. Hagman, Resistance measurements to find high moisture content inclusions adapted for large timber bridge cross-sections, BioResources 12 (2) (2017) 3570–3582.

[13] H. Li, M. Perrin, F. Eyma, X. Jacob, V. Gibiat, Moisture content monitoring in glulam structures by embedded sensors via electrical methods, Wood Science and Technology 52 (3) (2018) 733–752.

[14] EN13183-2, Moisture content of a piece of sawn timber–part 2: Estimation by electrical resistance method (2002).

[15] A. J. Stamm, The electrical resistance of wood as ameasure of its moisture content, Industrial & Engineering Chemistry 19 (9) (1927) 1021–1025.

[16] N. Björngrim, O. Hagman, X. A. Wang, Moisture content monitoring of a timber footbridge, BioResources 11 (2) (2016) 3904–3913.

[17] P. Dietsch, S. Franke, B. Franke, A. Gamper, S. Winter, Methods to determine wood moisture content and their applicability in monitoring concepts, Journal of Civil Structural Health Monitoring 5 (2) (2015) 115–127.

[18] B. Franke, S. Franke, M. Schiere, A. Müller, Moisture diffusion in wood–experimental and numerical investigations, in: World Conference on Timber Engineering, 2016.

[19] A. Blondel, M. Schmutz, M. Franceschi, F. Tichané, M. Carles, Temporal evolution of the geoelectrical response on a hydrocarbon contaminated site, Journal of Applied Geophysics 103 (2014) 161–171.

[20] A. Samouëlian, G. Richard, I. Cousin, R. Guerin, A. Bruand, A. Tabbagh, Three-dimensional crack monitoring by electrical resistivity measurement, European Journal of Soil Science 55 (4) (2004) 751–762.

[21] S. Barde-Cabusson, X. Bolós, D. Pedrazzi, R. Lovera, G. Serra, J. Martí, A. Casas, Electrical resistivity tomography revealing the internal structure of monogenetic volcanoes, Geophysical Research Letters 40 (11) (2013) 2544–2549.

[22] C. Verdet, Y. Anguy, C. Sirieix, R. Clément, C. Gaborieau, On the effect of electrode finiteness in small-scale electrical resistivity imaging, Geophysics 83 (6) (2018) EN39–EN52.

[23] M. Loke, R. Barker, Practical techniques for 3d resistivity surveys and data inversion1, Geophysical prospecting 44 (3) (1996) 499–523.

[24] R. Du Plooy, S. P. Lopes, G. Villain, X. Derobert, Development of a multi-ring resistivity cell and multi-electrode resistivity probe for investigation of cover concrete condition, NDT & E International 54 (2013) 27–36.

[25] J. Lataste, M. Behloul, D. Breysse, Characterisation of fibres distribution in a steel fibre reinforced concrete with electrical resistivity measurements, Ndt & E International 41 (8) (2008) 638–647.

[26] J. Priou, Y. Lecieux, M. Chevreuil, V. Gaillard, C. Lupi, D. Leduc, E. Rozière, R. Guyard, F. Schoefs, In situ dc electrical resistivity mapping performed in a reinforced concrete wharf using embedded sensors, Construction and Building Materials 211 (2019) 244–260. doi:https://doi.org/10.1016/j.conbuildmat.2019.03.152.

[27] Z. Luo, Z. Deng, K. Singha, X. Zhang, N. Liu, Y. Zhou, X. He, H. Guan, Temporal and spatial variation in water content within living tree stems determined by electrical resistivity tomography, Agricultural and Forest Meteorology 291 (2020) 108058.

[28] L. Martin, H. Cochard, S. Mayr, E. Badel, Using electrical resistivity tomography to detect wetwood and estimate moisture content in silver fir (abies alba mill.), Annals of Forest Science 78 (3) (2021) 1–17.

[29] D. Bieker, R. Kehr, G. Weber, S. Rust, Non-destructive monitoring of early stages of white rot by trametes versicolor in fraxinus excelsior, Annals of Forest Science 67 (2) (2010) 210.

[30] A. Ganthaler, J. Sailer, A. Bär, A. Losso, S. Mayr, Noninvasive analysis of tree stems by electrical resistivity tomography: unraveling the effects of temperature, water status, and electrode installation, Frontiers in plant science (2019) 1455.

[31] Neo-Terra, Ecological and energy transition in nouvelle-aquitaine region, `https://www.neo-terra.fr/` (2019).

[32] A. Kulkarni, K. Satyanarayana, P. Rohatgi, Electrical resistivity and dielectric strength of plant fibres, Journal of Materials Science 16 (6) (1981) 1719–1726.

[33] W. Hafsa, N. Angellier, M. Takarli, O. Pop, A mixed experimental–numerical electrical resistivity-based method for moisture content assessment in wood tested using the example of douglas fir, Wood Science and Technology 55 (3) (2021) 697–718. doi:https://doi.org/10.1007/s00226-021-01281-x.

[34] W. Hafsa, Approche expérimentale-numérique basée sur la résistivité électrique pour l'évaluation de l'état hydrique du douglas-fir, Ph.D. thesis, Limoges (2021).

[35] P. Perré, A. Degiovanni, Simulation par volumes finis des transferts couplés en milieux poreux anisotropes: séchage du bois à basse et à haute température, International Journal of Heat and Mass Transfer 33 (11) (1990) 2463–2478.

[36] B. Lasserre, Modélisation thermo-hygro-mécanique du comportement différé de poutres de structure en bois, Ph.D. thesis, Bordeaux 1 (2000).

[37] S. Merakeb, F. Dubois, C. Petit, Modeling of the sorption hysteresis for wood, Wood science and technology 43 (7) (2009) 575–589.

[38] H. N. Rosen, Exponential dependency of moisture diffusion coefficient, Wood science 8 (3) (1976) 174–179.

[39] J. Y. Liu, W. T. Simpson, Inverse determination of diffusion coefficient for moisture diffusion in wood, in: Proceedings of 33rd ASME national heat transfer conference: heat and mass transfer in porous media, August, 1999, pp. 15–17.

[40] Q. Zhou, Y. Cai, Y. Xu, X. Zhang, Determination of moisture diffusion coefficient of larch board with finite difference method, BioResources 6 (2) (2011) 1196–1203.

[41] J. A. Nelder, R. Mead, A simplex method for function minimization, The computer journal 7 (4) (1965) 308–313.

[42] J. C. Lagarias, J. A. Reeds, M. H. Wright, P. E. Wright, Convergence properties of the nelder–mead simplex method in low dimensions, SIAM Journal on optimization 9 (1) (1998) 112–147.

[43] C. T. Kelley, Iterative methods for optimization, SIAM, 1999.

[44] CEA, CAST3M finite element software, `www-cast3m.cea.fr` (2017).

[45] D. W. Marquardt, An algorithm for least-squares estimation of nonlinear parameters, Journal of the society for Industrial and Applied Mathematics 11 (2) (1963) 431–441.

[46] E. Agoua, S. Zohoun, P. Perré, A double climatic chamber used to measure the diffusion coefficient of water in wood in unsteady-state conditions: determination of the best fitting method by numerical simulation, International Journal of Heat and Mass Transfer 44 (19) (2001) 3731–3744.

[47] T. A. Nguyen, Approches expérimentales et numériques pour l'étude des transferts hygroscopiques dans le bois, Ph.D. thesis, Limoges (2014).

[48] H. Yamamoto, H. Sakagami, Y. Kijidani, J. Matsumura, Dependence of microcrack behavior in wood on moisture content during drying, Advances in Materials Science and Engineering 2013 (2013).

[49] A. J. Stamm, The fiber-saturation point of wood as obtained from electrical conductivity measurements, Industrial & Engineering Chemistry Analytical Edition 1 (2) (1929) 94–97.

[50] W. L. James, Electric moisture meters for wood, Vol. 8, US Department of Agriculture, Forest Service, Forest Products Laboratory, 1963.

[51] C. Carll, A. TenWolde, Accuracy of wood resistance sensors for measurement of humidity, Journal of Testing & Evaluation 24 (3) (1996) 154–160.